

**On the generation mechanisms of fluid-driven seismic signals related to volcano
tectonics**

Marco Fazio¹, Philip M. Benson¹ and Sergio Vinciguerra²

1) Rock Mechanics Laboratory, University of Portsmouth, Portsmouth, PO1 3QL, UK.

2) Department of Earth Sciences, University of Turin, 10125 Italy

Corresponding author: Marco Fazio, University of Portsmouth, Burnaby Building, Burnaby
Road, Portsmouth, PO1 3QL, UK. (marco.fazio@port.ac.uk)

Key points

- Fluid decompression tests in triaxially deformed Etna basalt test.
- Use of Acoustic Emission sensors to monitor fluid-induced micro-seismicity.
- Characteristic spectra of fluid driven seismic activity controlled by the number of phase sand pore pressure evolution.

This article has been accepted for publication and undergone full peer review but has not been through the copyediting, typesetting, pagination and proofreading process which may lead to differences between this version and the Version of Record. Please cite this article as doi: 10.1002/2016GL070919

Abstract

The generation mechanics of fluid-driven volcano seismic signals, and their evolution with time, remains poorly understood. We present a laboratory study aiming to better constrain the time evolution of such signals across temperature conditions 25 to 175°C in order to simulate a “bubbly liquid”. Simulations used pressures equivalent to volcanic edifices up to 1.6 km in depth using a triaxial deformation apparatus equipped with an array of Acoustic Emission (AE) sensors. We investigate the origin of fluid driven seismic signals by rapidly venting the pore pressure through a characterized damage zone. During the release of water at 25°C broadband signals were generated, with frequencies ranging from 50 to 160 kHz. However the decompression of a water/steam phase at 175°C generated a bi-modal spectrum of different signals, in the range 100 kHz and 160 kHz. These new results are consistent with natural signals from active volcanoes, such as Mt. Etna, and highlight the role of fluid and gas phases (such as “bubbly liquids”) in generating different types of volcano-tectonic seismicity.

Index terms

7280 Volcano seismology (4302, 8419)

8488 Volcanic hazards and risks (4302, 4328, 4333)

8419 Volcano monitoring (4302, 7280)

Keywords

Acoustic Emissions, Triaxial experiments, Decompression experiments, Fluid-induced seismicity, Fluid phases, Tremor

Introduction

Seismicity is the short-term precursory phenomenon most frequently detected before volcanic unrest, occurring as the Earth's crust is fractured as magma moves its way to the surface, and as fluids move within the faulted rock. Although different local terminologies have been widely used in the past [e.g. McNutt, 1996; Chouet, 1996; Neuberg, 2000; McNutt, 2005], according to Chouet [1996] volcano seismicity is defined in general terms of signal frequency or period.

Low frequency (LF), also known as long period (LP), events are characterized by a low harmonic frequency (0.5 – 5 Hz, Alparone et al., 2010) waveform lasting several seconds and a highly emergent onset that is difficult to identify. In contrast, high frequency events generated by deformation/failure mechanisms within the volcanic edifice are generally recorded in the frequency range of up to 15 Hz, termed volcano-tectonic (VT) events and feature an impulsive onset, a short broadband coda and higher energies. Between these two end-members, so-called hybrid events share features from both VT and LF activity: an impulsive onset followed by a lower frequency coda. Volcanic tremor show similar frequency content with respect to LP, but in a quasi-continuous signal that can last from minutes to months. Finally, very-low frequency (VLF, 0.3-0.01 Hz), also known as Very-Long Period (VLP), events have also been recorded since the deployment of broadband instruments in the 1990s [McNutt, 2005]. These signals share the harmonic behaviour of LPs and tremor, but at lower frequency.

The similarities between VLF, LF and tremor suggest a common source process. For this reason, seismic signals may be grouped into (1) VLF, LF and tremor likely generated as the result of fluid movement in fluid-filled cracks, and (2) VT events originated from shear/tensile mechanisms occurring in the solid rock. Crucially from a hazard and risk perspective, the interplay between VLF, LF, tremor and VT signals is diagnostic for understanding the fundamental magmatic processes within the volcanic structure, and in particular to the pressurisation of the volcanic plumbing system [e.g. Chouet & Matoza, 2013]. However, whilst great progress linking the underpinning geophysics to the families of seismic activity have been made over the past 20 years [e.g. Chouet 1996; 2003; McNutt, 2005, Chouet & Matoza, 2013], the physical source of tremor, LF and VLF events remains controversial. In particular, our knowledge of fluid/gas flow (decompression) rates needed to generate such signals and the coupling between different phases with respect to two-phases fluids such as “bubbly liquids” [e.g. Kumagai & Chouet, 2001], is lacking.

A key link is the causal relationship between LF events and tremor [Neuberg, 2000; Saccorotti et al., 2007]. Neuberg [2000] found that individual LF events at Soufrière Hills volcano (Montserrat) were linked to small-size, repetitive, non-destructive source areas which then merged into tremor before lava dome collapses. Later work by Saccorotti et al. [2007] distinguished two different seismic signals (LP and VLP) at Mt Etna volcano (Italy) during non-eruptive periods and interpreted the shallow plumbing system in terms of the resonance of a fluid-filled buried cavity. However, as these processes cannot be directly observed numerous models have been developed, often considering a fluid moving through a crack/damage network. In such an approach, the rapid fluid flow generates resonance within the crack [Julian, 1994], that is detected as a seismic event [e.g. Chouet, 1996, 2003]. Other generation mechanisms for the measured seismicity includes brittle failure of magma at its

glass transition point [Tuffen & Dingwell, 2005; Neuberg et al., 2006] and ‘stick-slip’ during the extrusion of solidifying lava [Iverson et al., 2006; Kendrick et al., 2014]. Of these, the fluid-filled crack model is the most common [Chouet & Matoza, 2013], where LF events are generally viewed as the response of the system to a sudden transitory pressure or fluid flow event, whilst tremor is generated by supported pressure fluctuations [Chouet, 1996]. Assuming the fluid is actively involved, the occurrence of low-frequency seismicity is considered to be a sign of pressurization in a magmatic/hydrothermal system, generating LF seismic activity that is, in turn, related to the rate and magnitude of pressurisation and to the intensity of explosive activity [Chouet, 1996].

In this study we investigate the change in micro-seismic signal frequency as it evolves from tremor to LF by releasing high pressure, high temperature fluid (water) from a pre-faulted sample of basalt from Mt Etna, recording the induced seismicity via Acoustic Emission (AE) analysis [e.g. Burlini et al., 2007]. This is the laboratory analogue for field scale seismicity and is widely used in rock physics experiments [e.g. Benson et al., 2007, 2010]. While the vast majority of AE studies have focused on the nucleation and propagation of shear faulting analogous to VT and due to rupture processes that precede and accompany the formation of a major damage zone in a centimetres-scale rock specimen [e.g. Ohnaka and Mogi, 1982; Read et al., 1995; Benson et al., 2007], a more limited dataset is available for the fluid-induced seismicity [e.g. Burlini et al., 2007; Benson et al., 2008; 2010; 2014]. In particular these early studies of fluid (water) induced AE have concentrated to date on water at ambient temperature conditions. Here we report new data taken from a more systematic study in order to better understand the subtle links between fluid phase on the character (frequency) of generated AE, linking these data to the statistics of the events in time and space. This is

important, as the laboratory calibrations of these subtle effects are crucial for quantitative interpretation of field scale data.

The key advantage of performing laboratory experiments is that conditions of pressure and temperature at which AE events occur are known and well controlled. Although real volcanic conditions act on different time and space scales and are different in terms of heterogeneity, the use of laboratory rock physics as a proxy for the microseismic source has shown to be a useful tool in reproducing the fundamental processes and the corresponding geophysical signatures at controlled stress conditions [e.g. Read et al., 1995; Sammonds, 1999; Burlini et al., 2007; Benson et al., 2008]. It is also well established that the physical processes generating the laboratory AEs and those responsible for the volcanic earthquake are similar and scalable [e.g. Aki & Richards, 1980; Burlini et al., 2007; Benson et al., 2010]. Appropriate scaling approaches for centimetre-scale rock samples to a kilometre-scale volcanic edifice continue to be debated, however, basic qualitative interpretations can be made by considering similarities between laboratory and field waveforms/spectra, and quantitatively by taking the size – frequency relationship [Burlini et al., 2007; Benson et al., 2010]. We hereafter report a suite of new experiments where we generated and analysed seismic signals during the decompression of single- and dual-phase fluids under controlled temperature and confining pressure conditions.

Material investigated and Experimental procedures

The sample material was an alkali, porphyritic basalt from Mt Etna (Italy) with density $2870 \pm 10 \text{ kg/m}^3$ and porosity $2.02 \pm 0.12\%$. Cylindrical samples of 100 mm (length) by 40 mm (diameter) were drilled using a standard diamond tipped coring drill. In addition, a conduit of 3 mm is drilled through the centre of the long axis to enable pore fluid (water) to access the eventual damage zone. Experiments were carried out using an externally heated, servo-controlled triaxial apparatus (Fig. S1) at a confining pressure of 46 MPa and pore pressure of 16 MPa, yielding an effective pressure of 30 MPa and broadly representative of volcanic conditions and shallow plumbing systems at approximately 1.6 km depth. Standard triaxial deformation experiments were performed at a constant strain rate of 10^{-5} s^{-1} , in order to generate a shear/damage zone oriented at approximately 30° with respect to the loading. Once this shear zone and the associated damage zone are created the maximum principal stress is then reduced to yield a hydrostatic stress condition (and therefore lock the fault). At this stage one of two protocols is followed, either i) the external furnace increases sample temperature (and pore fluid temperature to 175°C), or ii) the temperature is held constant at approximately 25°C . After this, in both cases, through a fast-acting solenoid valve connected to the lower end of the sample the pore fluid pressure is rapidly released to atmosphere via the rapid fluid flow from the established damage zone.

An array of 12 Lead Zirconate Titanate (PZT) sensors (6 at 1 MHz-central frequency and 6 at 200 kHz), embedded within an engineered Nitrile jacket [Sammonds, 1999], is used to compute P-wave elastic velocities. This consists of ‘pulsing’ sensors in sequence, with the remaining sensors recording the arrival of the signal via the time-of-flight method [Pettitt, 1998] and to derive a velocity model necessary for the location algorithm. A downhill simplex method [Nelder & Mead, 1965; Press et al., 1994] is used to locate the micro-seismic

(AE) events, extracted from the continuous signal, (which we term *streaming data*) recorded by 8 of the 12 channels. The streaming data is processed offline after the experiment allowing events to be “harvested” from this streamed waveform. Before being recorded, all signals are pre-amplified by dual 30 dB buffered amplifiers, which also incorporate a band-pass filter 10 kHz – 1 MHz to remove local noise. In this study, the use of lower frequency sensors allows for a more robust statistics when analysing the fluid-induced (LF) AE data.

During the experiment, axial stress and pore fluid pressures are recorded via high speed data acquisition systems. This enables the character and the frequency of the AE to be compared to the axial stress/pore pressure change, as a function of time.

Results

A series of 7 experiments were performed (here shown the experiments with the best signal-to-noise ratio, SNR), with peak stress at failure measured between 436 and 465 MPa. After failure a stress drop of approximately 250 MPa is measured (Fig. S2), with post-test inspection revealing the classic shear fracture at 30° to the σ_1 direction. This part of the experiment generates a shear fault accessed by the central conduit. An instantaneous pore pressure release (hereafter called “venting”) is then performed by discharging the pore fluid from the bottom of the sample via a solenoid valve and recording the pore pressures at high data acquisition rates of 5 kHz.

We find that the pore pressure decay follows a different path depending on sample temperature (Fig. 1). At 25°C (experiment EB25) the lower pore pressure decreases instantaneously to zero (Fig. 1a, solid green line), as it is directly connected to the solenoid valve. Meanwhile, the top pore pressure decays over a period of two minutes (Fig. 1a, solid black line). At elevated temperatures of 175°C (experiment EB175), both bottom and top pressure decays quickly to approximately 1.5 MPa (Fig. 1b, solid lines), followed by a more gentle decrease to 0.9 MPa over the following 10 seconds. Both pressures stabilize at this value over a period of 70 seconds, after which the bottom pore pressure decrease to 0.2 MPa. During the two minutes after the venting, the maximum cumulative AE hits (AE counts above a fixed threshold) occurs during the main venting stage (around 1350 and 1500 cumulative hits in the first second in EB25 and EB175 respectively, Fig. 1a, 1b, dashed red lines). At 25 °C, 10 seconds after the release, the cumulative hits sharply increase up to a value of 1800 hits, while in the following 110 seconds cumulative AE hits increase at a slower rate reaching a total of 1900 at 120 s (Fig. 1a). At 175 °C a similar behaviour is seen: after the initial peak, the cumulative hit rate steadily increased up to 1800 hits (Fig. 1b).

Figure 1 shows a 58 ms segment around the initial pore pressure decay (Fig. 1c, 1d, thick black and green lines), for both the raw streaming data waveform (Fig. 1c, 1d, thin blue lines) and its frequency-power spectrogram (Fig. 1e, 1f) of that AE activity as a function of time during venting. In EB25, the onset of a tremor-like AE activity occurred 12 ms after the release, with a duration of 10 ms (Fig. 1c). Conversely, in EB175 the AE activity started 4 ms after the release. This AE tremor had a much longer duration (30 ms) than the tremor generated in EB25. In terms of frequency, for experiment EB25 we measured a broadband tremor with frequency ranging from 40 kHz to 200 kHz (Fig. 1e), whereas for experiment EB175 a continuous spectrum was measured instead with frequency ranging between 100 kHz and 160 kHz (Fig. 1f).

To further investigate this frequency switch, a systematic statistical analysis was developed. This consisted of extracting a sequence of 819.2 μs -long events from EB25 (56 events) and EB175 (31 events) in the 120 seconds following the venting. In each signal, the initial onset time was picked and a FFT analysis was performed over a 102.4 μs -long window in order to obtain a characteristic frequency of the AE. This permits the dominant frequency of each event to be superimposed on the pore pressure decay (Fig. 2a and 2b). In general, we note that the dominant frequencies generated at 25°C fails within the frequency range 40-160 kHz (Fig. 2a), whereas at 175°C two subtle ranges of dominant frequency emerge: 90-110 kHz and 160-180 kHz (Fig. 2b). This analysis has been performed on the other 5 experiments, which resulted in analogous results (Fig. S3).

To evaluate the extent of the broadband feature in EB25 and of the bi-modality in EB175, we use a cross-correlation analysis on the event waveforms in each experiment. The method cross-correlates the waveforms between events, resulting in a matrix of cross-correlation coefficients. Choosing a threshold of 0.7, we then define a master event, corresponding to the event with the highest number of correlated event. For each of the correlated events, a spectrum over the same time window of 102.4 μs has been calculated and finally, these spectra are stacked, resulting in the plots shown in Figure 2c, d. In EB25, 15 events are correlated and the stacked spectrum has a broadband feature, with 9 of these events being classified as broadband. In EB175, 12 events are correlated, displaying a well-defined bi-modality with narrower spectral peaks, with 7 of these events classified as bi-modal.

Figures 3a and 3c show a spectral analysis of these waveforms for the two master spectra and their waveforms occurring in EB25 and EB175. When the streaming data is harvested into discrete events, a range of broadband and bi-modal features are observed during the tremor-like AE activity, depending on the P/T conditions. In EB25 the amplitude spectrum lies constantly above the -6 dB threshold from 80 to 145 kHz (Fig. 3a). Conversely in EB175 only two narrow frequency ranges lie above the -6 dB threshold: 80 – 105 kHz and 150 – 180 kHz (Fig. 3c).

Finally, AE focal mechanisms were calculated. Due to the low amplitude, low SNR and low number of picks available (just 8 channels recorded streaming data), reasonable focal mechanisms were obtained for only 11 AEs harvested during the venting stage of both experiments (6 for EB25, 5 for EB175: Table S1). These 11 events show a component of Double Couple (DC) (ranging from 7% to 60%, with an average of 32%). The component of Compensated Linear Vector Dipole (CLVD) is slightly higher, ranging from 21% to 61% and with an average of 42%, reflecting the enhanced contribution of the fluid motion to the mechanism [e.g. Julian, 1994; Benson et al., 2008].

Discussion and conclusions

During our experiments we recorded AE events in the frequency range from 40 to 200 kHz. This is comparable to the field-scale volcanic seismic signals occurring at frequencies 0.1 – 10 Hz via simple frequency/scale relationship [Aki & Richards, 1980; Burlini et al., 2007; Benson et al., 2008; Browning et al., 2016]. LP and VLP signals with both uni-modal and bi-modal spectra have been observed at Mt. Etna on September 05, 2013 (Fig. 3b) and January 10, 2015 (Fig. 3d) respectively (recorded by INGV permanent seismic array operating at Mt Etna). The September 05 VLP event is characterized by a spectrum, with a single peak,

between 0.5 Hz and 2 Hz, lying above the -6 dB threshold and has been associated to the explosive activity at the New South-East Crater, which involves gas-rich erupted magma [Bonaccorso et al., 2014] and is typically accompanied by intense degassing at the nearby craters [Viccaro et al., 2015].

The January 10 LP signal instead shows a spectrum with two peaks above the -6 dB line, at 4-5 Hz and at 7.5 Hz, and has been linked to strombolian activity and ash emission at Voragine crater. We therefore notice the link between a mono-phase fluid (gas) and a single peak spectrum, while a double-phase fluid (liquid-gas) produces a two-peak spectrum. Bi-modal spectra have also been found at Stromboli volcano [SgROI et al, 2009] and interpreted as the overlap of deep magmatic fluids and shallower fluids enriched of gas. This is consistent with our findings, confirming the key role played by the type and number of phases forming the fluid to the character of the fluid-induced seismicity. Although the comparison between fluid-induced AE and volcanic LP and VLP signals has been previously postulated by Julian [1994] and shown qualitatively in the laboratory by Benson et al. [2008], in this work we expand this to better analyse the competition between gas and liquid due to elevated temperatures and with respect to pore pressure decompression in order to understand the relationship between the source and the corresponding signal. This is important, as whilst the basic mechanism for AE generation due to the rapid movement of water through a fractured zone (as the pore pressure is released) is known, the precise role of the pore fluid phase (water, bubbly liquids, etc.) that generates turbulence manifested as a sustained tremor (Fig. 1c, 1d) has yet to be constrained mainly due to the difficulties in generating low amplitude events with acceptable quality and build a catalogue in meaningful statistical terms.

To better understand the interactions between the rock matrix (damage zones) and the influence of pore fluids and pressure fluctuations, we have developed a suite of experiments to cover a wide spectrum of fluid phases and consider the dominant frequency of events to better understand the contribution of the pore fluid water/gas phases to the generated AE, and the distribution of these AE across their dominant frequencies as a function of time and fluid pressure (Fig. 2a, 2b). This is a key novelty with respect to previous early work that used the end members given by either fully fluid-saturated or dry rocks. For the events generated at 25°C, we obtained a fluid movement consisting of a single-phase liquid. Once the fluid is released a broadband tremor takes place followed by events with dominant frequencies widespread in the same frequency of the tremor, but characterized by a largely monochromatic spectrum, as shown in Fig. 2c. Conversely, at 175°C, well above the boiling temperature of water (at ambient pressure), a multi-phase system is generated by the venting with a liquid-gas mixture being released to ambient pressure. These two phases coexisted inside the sample, due to the significant gradient in pore pressure between the upper and the lower ends of the sample, likely generating a time-varying “bubbly-liquid” type of fluid. We interpret the resulting bi-modal AE event activity (with two clear dominant frequencies at 100 and 160 kHz) to be a consequence of a two-phase bubbly-fluid. This has previously been established as the source of low frequency activity, both in the laboratory and the field.

Quality factor (Q) analysis (Fig. S4), revealed lower Q for experiment with liquid water and higher Q when a “bubbly-liquid” is released, consistently with the model of Kumagai & Chouet [2000, 2001]. Kumagai and Chouet [2000, 2001] also postulated a higher frequency content for fluids richer in gas, which explains the 160 kHz cluster towards the end of the venting stage (Fig. 2b), where the gas-fraction is expected to be higher due to the continue transformation of superheated water into gas. The decrease in the amplitude ratio between the

spectral peak at 100 kHz and the spectral peak at 160 kHz (Fig. S5), points to the same direction (additional discussion in SI).

Examining the pore pressure curve in EB175 (Fig. 1d), further evidence for the presence of a two-phase fluid stems from the plateauing of top and bottom pressure at approximately 1 MPa. This is close to the stable equilibrium condition where liquid water exists (approximately 0.7 MPa) at 175°C. The small discrepancy (0.3 MPa) is likely to be due to the time lag due to the placement of the measuring transducers, located about 2 m (top pressure) and 1.5 m (bottom pressure) away from the sample itself. Furthermore, the re-expansion of the fluid and the establishment of equilibrium is then likely to impede the pore pressure decay and therefore the generation of AEs. This is supported by the occurrence of only 4 events during the first seconds of release (Fig. 1d), whilst some 27 events were recorded in the same time-window for the venting at 25°C (Fig. 1c). We also observed individual events of short duration (Fig. 3a, 3c) that we interpret as fluid-generated, due to the relatively low DC component (32%) and the similarity in the frequency content between these and their subsequent tremor. Both cases are consistent with a response to sudden pressure transient and sustained pressure fluctuations [e.g. Chouet, 1996].

The key findings of this study are: 1) to find a better defined role of pore pressure decay rate on the generation of AEs and how these transition from sustained tremor of tens of ms long to discrete events with similar spectral characteristics, but hundreds of μ s long; 2) the simulation and characterization of the role of phase changes in the pore fluid on the characteristic AE spectrum, determining subtle changes to the spectrogram depending on fluid phase mixture. Such an outcome has been theoretically postulated by Kumagai and Chouet [2000; 2001] who considered a range of different fluids within fracture damage zones

such as dusty gasses and bubbly fluids resonating through different crack geometries. Taken together our data provide new quantitative evidence for models linking low frequency signals in volcanic areas as due to the resonance of high-pressure fluid filled crack/cavities [e.g. Chouet, 1996]. We also suggest that low frequency events (tremor, LPs and VLPs) could be used to discriminate between different fluid-driven processes, ultimately helping eruption forecasting by characterizing the different supercritical fluids at depth, as well as providing better constraints on the emplacement mechanics within the volcanic edifice generally [Neuberg, 2000]. We find that the effects of the fluids phase/type on the AE data (and by extension, field seismic data) are very subtle, and so using such an analysis to infer deep magmatic plumbing systems should be done with caution.

Acknowledgements

The authors acknowledge Emily Butcher for technical support in the Rock Mechanics Laboratory, Prof. Philip Meredith (UCL) and Dr. Peter Rowley (UoP) for thoughtful discussions, Dr. Salvatore Alparone (INGV Catania) is especially acknowledged for providing the data from Mt Etna and useful discussions on field data. A special thanks also for the anonymous reviewer for his/her contribution through significant revisions. The data used are listed in the references, figure and supplements. This research was funded by a University Graduate Bursary grant to MF. The authors declare no competing interests.

References

- Aki, K., & Richards, P. G. (1980). Quantitative seismology: Theory and methods. *Vol II*.
- Benson, P. M., Thompson, B. D., Meredith, P. G., Vinciguerra, S., & Young, R. P. (2007). Imaging slow failure in triaxially deformed Etna basalt using 3D acoustic-emission location and X-ray computed tomography. *Geophysical research letters*, *34*(3).
- Benson, P. M., Vinciguerra, S., Meredith, P. G., & Young, R. P. (2008). Laboratory simulation of volcano seismicity. *Science*, *322*(5899), 249-252.
- Benson, P. M., Vinciguerra, S., Meredith, P. G., & Young, R. P. (2010). Spatio-temporal evolution of volcano seismicity: A laboratory study. *Earth and Planetary Science Letters*, *297*(1), 315-323.
- Benson, P. M., Vinciguerra, S., Nasser, M. H., & Young, R. P. (2014). Laboratory simulations of fluid/gas induced micro-earthquakes: application to volcano seismology. *Frontiers in Earth Science*, *2*, 32.
- Bonaccorso, A., Calvari, S., Linde, A., & Sacks, S. (2014). Eruptive processes leading to the most explosive lava fountain at Etna volcano: The 23 November 2013 episode. *Geophysical Research Letters*, *41*(14), 4912-4919.
- Browning, J., Meredith, P., & Gudmundsson, A. (2016). Cooling-dominated cracking in thermally stressed volcanic rocks. *Geophysical Research Letters*, *43*(16), 8417-8425.
- Burlini, L., Vinciguerra, S., Di Toro, G., De Natale, G., Meredith, P., & Burg, J. P. (2007). Seismicity preceding volcanic eruptions: New experimental insights. *Geology*, *35*(2), 183-186.
- Chouet, B. A. (1996). Long-period volcano seismicity: its source and use in eruption forecasting. *Nature*, *380*(6572), 309-316. doi:10.1038/380309a0
- Chouet, B. (2003). Volcano seismology. *Pure and Applied Geophysics*, *160*(3-4), 739-788.

Chouet, B. A., & Matoza, R. S. (2013). A multi-decadal view of seismic methods for detecting precursors of magma movement and eruption. *Journal of Volcanology and Geothermal Research*, 252, 108-175.

Iverson, R. M., Dzurisin, D., Gardner, C. A., Gerlach, T. M., LaHusen, R. G., Lisowski, M., Major, J. J., Malone, S. D., Messerich, J. A., Moran, S. C., Pallister, J. S., Qamar, A. I.,

Schilling S. P. & Wallace, J. W. (2006). Dynamics of seismogenic volcanic extrusion at Mount St Helens in 2004–05. *Nature*, 444(7118), 439-443.

Julian, B.R.(1994), Volcanic tremor: Non-linear excitation by fluid flow: *J. Geophys. Res.*, v. 99, p. 11,859–11,877, doi: 10.1029/93JB03129.

Kendrick, J. E., Lavallée, Y., Hirose, T., Di Toro, G., Hornby, A. J., De Angelis, S., & Dingwell, D. B. (2014). Volcanic drumbeat seismicity caused by stick-slip motion and magmatic frictional melting. *Nature Geoscience*, 7(6), 438-442.

Kumagai, H., & Chouet, B. A. (2000). Acoustic properties of a crack containing magmatic or hydrothermal fluids. *Journal of Geophysical Research: Solid Earth*, 105(B11), 25493-25512.

Kumagai, H., & Chouet, B. A. (2001). The dependence of acoustic properties of a crack on the resonance mode and geometry. *Geophysical research letters*, 28(17), 3325-3328.

McNutt, S. R. (1996). Seismic monitoring and eruption forecasting of volcanoes: a review of the state-of-the-art and case histories. In *Monitoring and mitigation of volcano hazards* (pp. 99-146). Springer Berlin Heidelberg.

McNutt, S. R. (2005). Volcanic seismology. *Ann. Rev. Earth planet. Sci.*, 32, 461-491.

Nelder, J. A., & Mead, R. (1965). A simplex method for function minimization. *The computer journal*, 7(4), 308-313.

Neuberg, J. (2000). Characteristics and causes of shallow seismicity in andesite volcanoes. *Philosophical Transactions of the Royal Society of London. Series A: Mathematical, Physical and Engineering Sciences*, 358(1770), 1533-1546.

Neuberg, J. W., Tuffen, H., Collier, L., Green, D., Powell, T., & Dingwell, D. (2006). The trigger mechanism of low-frequency earthquakes on Montserrat. *Journal of Volcanology and Geothermal Research*, 153(1), 37-50.

Ohnaka, M., & Mogi, K. (1982). Frequency characteristics of acoustic emission in rocks under uniaxial compression and its relation to the fracturing process to failure. *Journal of Geophysical Research: Solid Earth (1978–2012)*, 87(B5), 3873-3884.

Pettitt, W. S. (1998). *Acoustic emission source studies of microcracking in rock* (Doctoral dissertation, University of Keele).

Press, W. H., Flannery B. P., Teukolsky S. A., & Vetterling W. T. (1994). *Numerical Recipes in C: The Art of Scientific Computing*, 2nd edition, Cambridge University Press, Cambridge.

Read, M. D., Ayling, M. R., Meredith, P. G., & Murrell, S. A. (1995). Microcracking during triaxial deformation of porous rocks monitored by changes in rock physical properties, II. Pore volumetry and acoustic emission measurements on water-saturated rocks. *Tectonophysics*, 245(3), 223-235.

Saccorotti, G., Lokmer, I., Bean, C. J., Di Grazia, G., & Patanè, D. (2007). Analysis of sustained long-period activity at Etna Volcano, Italy. *Journal of volcanology and geothermal research*, 160(3), 340-354.

Sammonds, P. R. (1999). Understanding the fundamental physics governing the evolution and dynamics of the Earth's crust and ice sheets. *Philosophical Transactions of the Royal Society of London. Series A: Mathematical, Physical and Engineering Sciences*, 357(1763), 3377-3401.

Sgroi, T., Montuori, C., Agrusta, R., & Favali, P. (2009). Low-frequency seismic signals recorded by OBS at Stromboli volcano (Southern Tyrrhenian Sea). *Geophysical Research Letters*, 36(4).

Tuffen, H., & Dingwell, D. (2005). Fault textures in volcanic conduits: evidence for seismic trigger mechanisms during silicic eruptions. *Bulletin of Volcanology*, 67(4), 370-387.

Viccaro, M., Calcagno, R., Garozzo, I., Giuffrida, M., & Nicotra, E. (2015). Continuous magma recharge at Mt. Etna during the 2011–2013 period controls the style of volcanic activity and compositions of erupted lavas. *Mineralogy and Petrology*, 109(1), 67-83.

Accepted Article

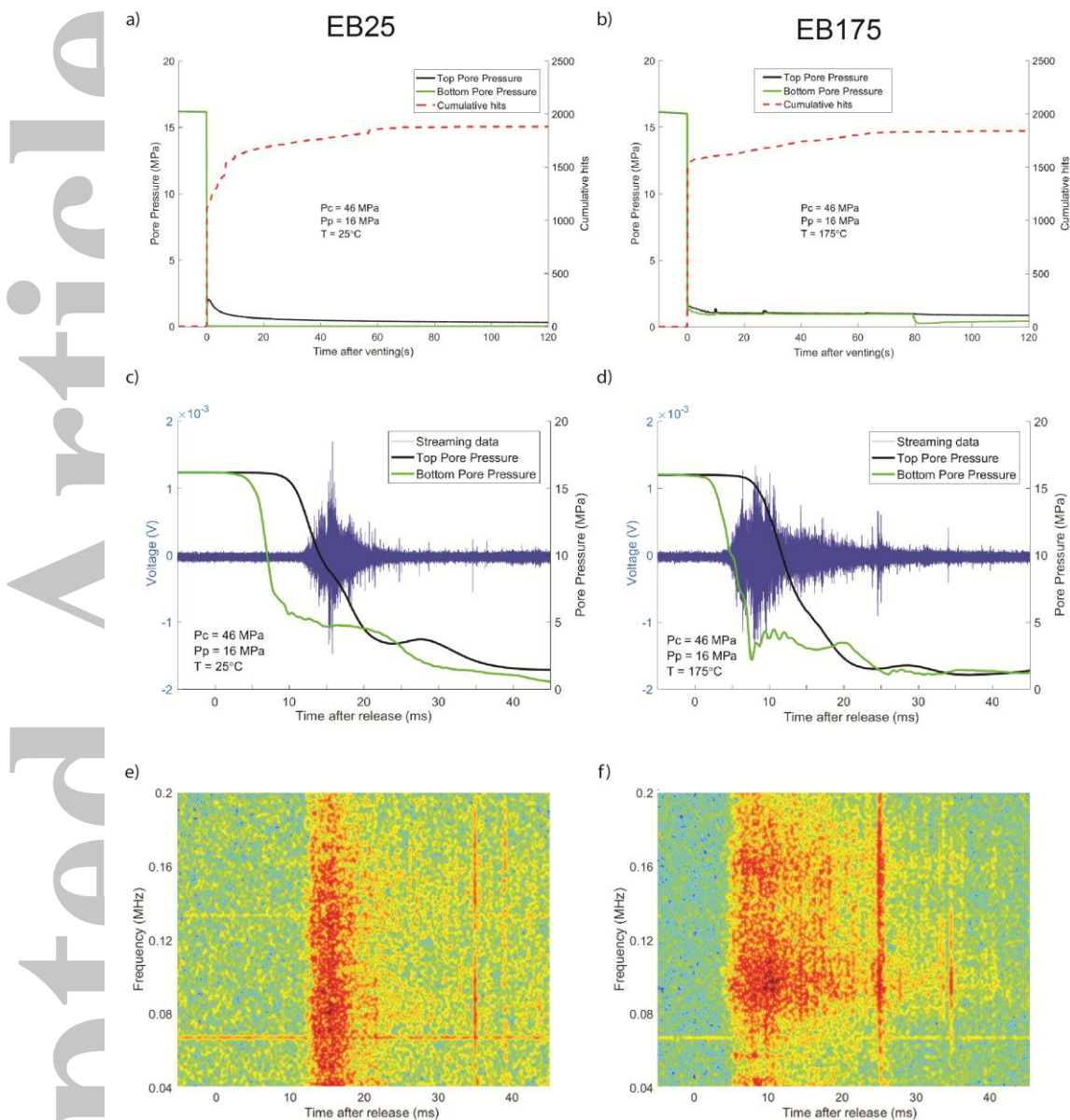


Figure 1: Top panels: venting stage for EB25 (a) and EB175 (b). Top (black) and bottom (green) pore pressure – time plot (left hand axis, solid lines) and cumulative hit rate (right hand axis, dashed red line). In EB25 (a) the top pore pressure decays quickly immediately after the release allowing further hits in the following 10 seconds, while fewer hits were recorded when the decrease was slower than the first part of the decay curve. In EB175, top and bottom pore pressure both stabilized at 0.9 MPa, with the hit rate steadily increasing throughout the one minute of observation.

Middle and bottom panels: a 58 millisecond-long snapshot of the continuous waveforms (c and d) and their spectrograms (e and f) when the pore fluid is vented out by the solenoid valve for EB25 and EB175 respectively. In c) and d) the thick black and green lines are top and bottom pore pressure respectively, while the thin blue line represent the streaming data. In e) and f), red denotes the higher amplitudes in the signal at that particular frequency and time, while green/blue represent lower amplitudes. At 25°C (e), a broadband tremor occurred, starting 12 ms after the release and lasting for 10 ms. At 175°C (f) the tremor starts 5 ms after the release and has a duration of 30 ms, with the power of the signal concentrated at few discrete frequencies, 100 and 160 kHz.

Accepted Article

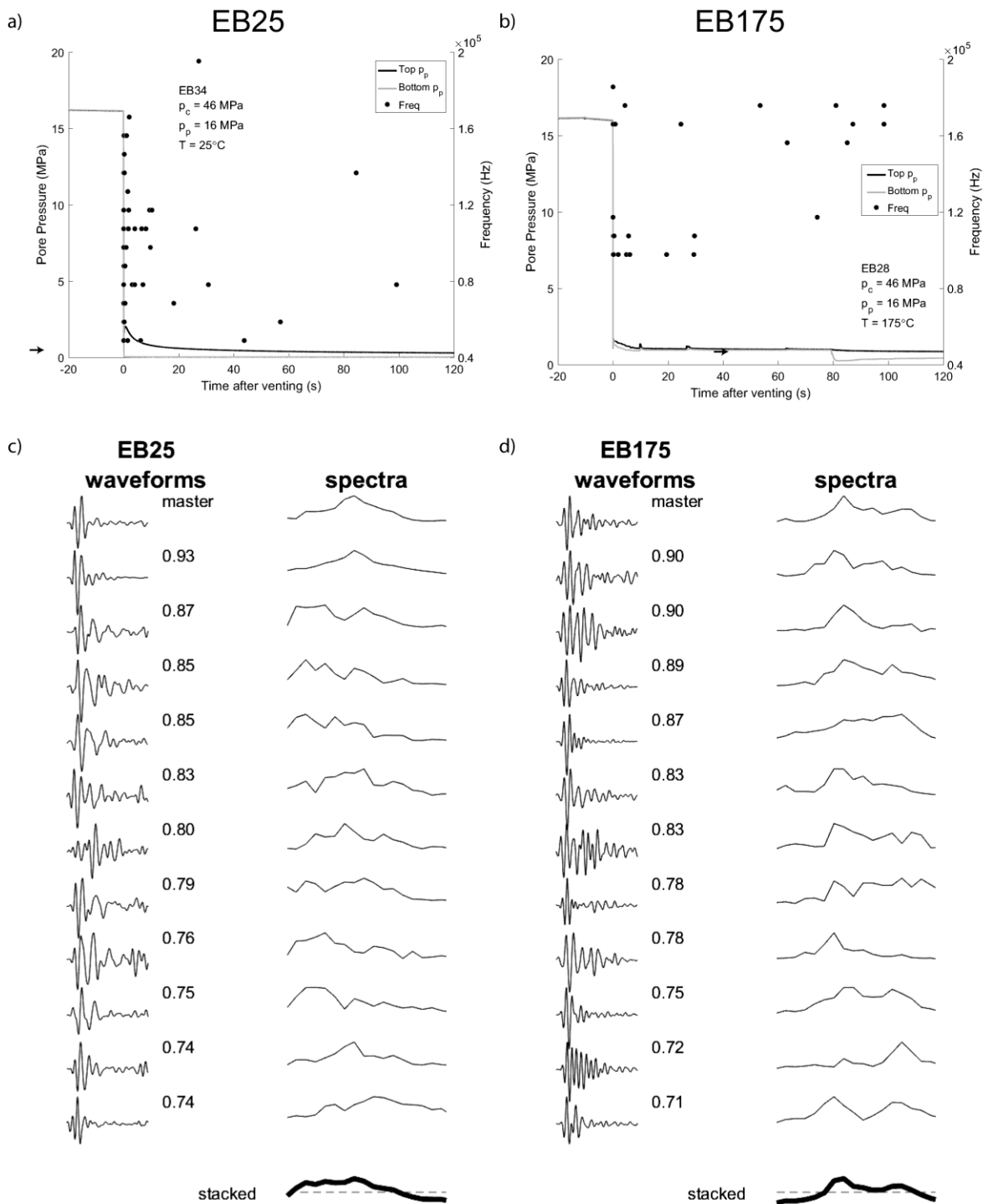


Figure 2: Panel (a) and (b) show the top (black) and bottom (grey) pore pressure – time plot (left hand axis, solid lines) with dominant event frequencies shown on the right hand axis (black filled circles) of the harvested events for EB25 and EB175 experiments respectively.

The arrows indicated the events shown in detail in Figure 3a and 3c. Panel (c) and (d)

represent the correlated waveforms and their spectra. The number on the waveform is the correlation coefficient with the master waveform. On the bottom right of each panel, the spectra, resulting from the stacking of the spectra of the correlated events is plotted, with the dashed horizontal line marking -6 dB level. While in EB25 a broadband spectrum characterizes the correlated events, the stacked spectrum in EB175 presents two peaks. These characteristics are similar to those observed for the tremors (Fig. 2c, 2d), suggesting that the number of phases in the fluid controls the spectrum of the AE activity.

Accepted Article

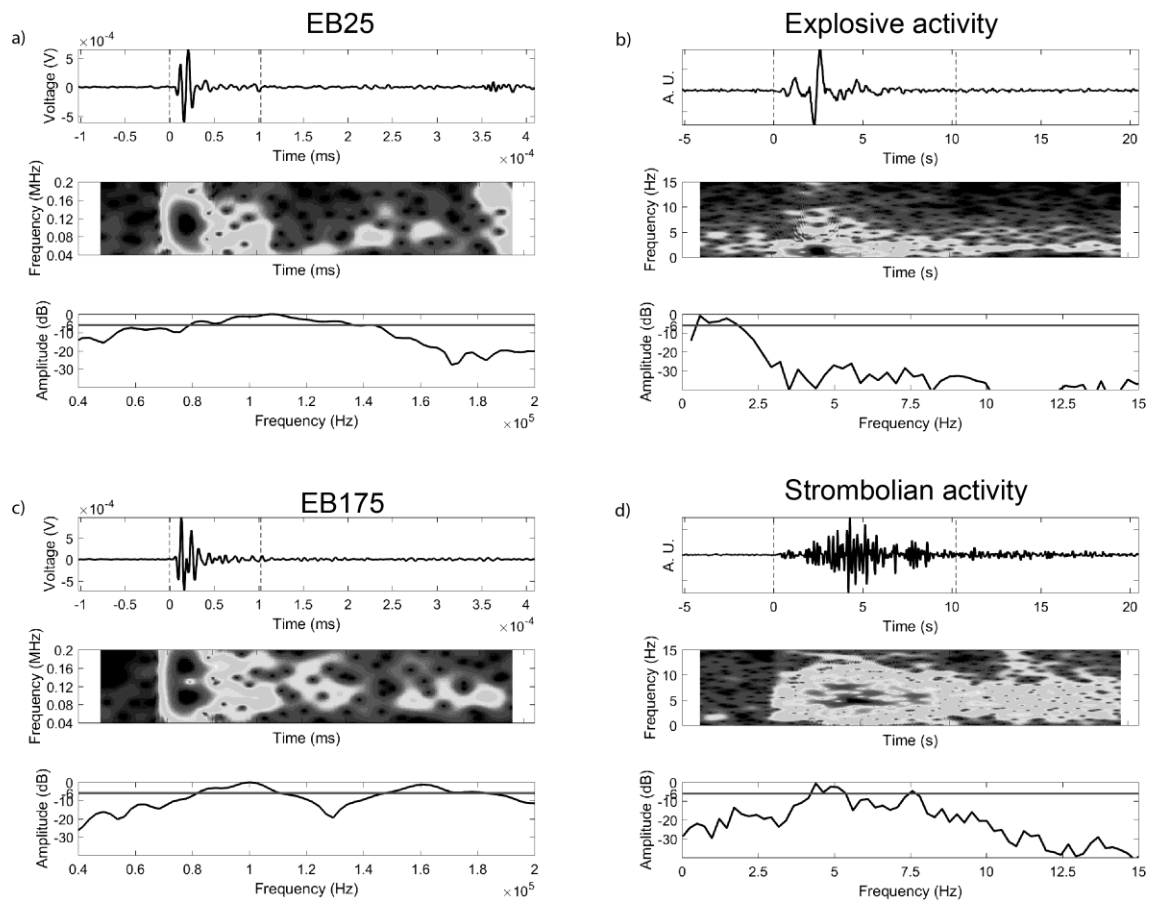


Figure 3: The laboratory signals of experiment EB25 (a) and EB175 (c) are matched with the field scale volcanic events (b, d). Each panel shows the waveforms (upper part), the spectrogram (middle) and the waveform spectral density (in dB units, lower part). The Fast Fourier Transform is calculated from the onset of the event over a 1024-point-long window (vertical dashed lines).

At 25°C (panel a), the event is characterized by a broadband spectrum with a frequency range of 80 – 145 kHz above the -6 dB threshold. This is somehow similar to the VLP event (panel b) recorded at Mt. Etna (Italy) on September 05, 2013, where a single peak (0.5 -2 Hz) above the -6 dB is present. This volcanic signals was recorded three minutes before mild explosive activity at the New South-East Crater. At 175°C two dominant frequency ranges appears above the -6 dB threshold: 80 – 105 kHz and 150 – 180 kHz (panel c). A similar bi-modality (first peak between 4.5 Hz and 5.5 Hz, second narrower peak at 7.5 Hz) has been observed in

the LP event (panel d) recorded at the same volcano on January 10, 2015. This LP signal was associated to the continuous strombolian activity and ash emission from the Voragine crater.

This volcanic activity is marked by the simultaneous presence of both liquid and gas phases.

Field scale events come from INGV seismic network.

Accepted Article